0888-8809/07/$15.00/0
Printed in U.S.A.

Molecular Endocrinology 21(9):2255–2269

doi: 10.1210/me.2007-0077

Regulated Autophagy Controls Hormone Content in Secretory-Deficient Pancreatic Endocrine β-Cells

Brad J. Marsh, Chad Soden, Cristina Alarcón, Barton L. Wicksteed, Kazuro Yaekura, Adam J. Costin, Garry P. Morgan, and Christopher J. Rhodes

Institute for Molecular Bioscience (B.J.M., A.J.C., G.P.M.), Queensland Bioscience Precinct, The University of Queensland, Brisbane, Queensland 4072, Australia; The Kovler Diabetes Center (C.S., C.A., B.L.W., K.Y., C.J.R.), Department of Medicine, Section of Endocrinology, Diabetes, and Metabolism, University of Chicago, Chicago, Illinois 60637

Endocrine cells are continually regulating the balance between hormone biosynthesis, secretion, and intracellular degradation to ensure that cellular hormone stores are maintained at optimal levels. In pancreatic β-cells, intracellular insulin stores in β-granules are mostly upheld by efficiently up-regulating proinsulin biosynthesis at the translational level to rapidly replenish the insulin lost via exocytosis. Under normal circumstances, intracellular degradation of insulin plays a relatively minor janitorial role in retiring aged β-granules, apparently via crinophagy. However, this mechanism alone is not sufficient to maintain optimal insulin storage in β-cells when insulin secretion is dysfunctional. Here, we show that despite an abnormal imbalance of glucose/glucagon-like peptide 1 regulated insulin production over secretion in Rab3A$^{-/-}$ mice compared with control animals, insulin storage levels were maintained due to increased intracellular β-granule degradation. Electron microscopy analysis indicated that this was mediated by a significant 12-fold up-regulation of multigranular degradation vacuoles in Rab3A$^{-/-}$ mouse islet β-cells ($P \leq 0.001$), which by further electron microscopy-tomography analysis was found to be mostly contributed by microautophagic activity. This increased autophagic activity in Rab3A$^{-/-}$ mouse islet β-cells was associated with a specific decrease in islet lysosomal-associated membrane protein 2 gene expression ($P \leq 0.05$), at both the mRNA and protein expression levels. Lysosomal-associated membrane protein 2 is a documented negative regulator of autophagy. These findings indicate that the up-regulation of degradative pathways provides secretory-deficient endocrine cells with a compensatory mechanism for regulating their intracellular hormone content *in vivo*. These data may also have implications for the β-cell's response to diminished insulin secretion during the pathogenesis of type 2 diabetes. (*Molecular Endocrinology* 21: 2255–2269, 2007)

THE PANCREATIC β-CELL has typical endocrine cell characteristics, in that its primary polypeptide hormone product (insulin) is packaged into large membrane-bound secretory vesicles (β-granules) at the *trans*-face of the Golgi complex for release via the regulated secretory pathway (1). Most β-granules reside in an internal storage pool, but in response to a physiological stimulus such as elevated blood glucose, a subpopulation of these granules are transported to plasma membrane and undergo exocytosis, resulting in the extracellular secretion of insulin (2). Although relatively few β-granules are actually exocytosed in response to glucose, the insulin secreted from the β-cell is rapidly replenished by a specific glucose-induced increase in proinsulin biosynthesis (3). Under normal circumstances, *i.e.* after short-term glucose stimulation (<4 h), proinsulin synthesis occurs exclusively at the translational level. However, this is supplemented by additional up-regulation of preproinsulin gene transcription with chronic exposure to glucose (>12 h) (3, 4). Despite their parallel regulation by glucose, insulin production and secretion are controlled by distinct mechanisms (3). For example, a difference between the threshold glucose concentration required to stimulate proinsulin biosynthesis (2–4 mM) *vs.* insulin secretion (4–6 mM) ensures that insulin production is maintained under conditions in which insulin secretion is negligible (5). This also indicates that the β-cell has a bias toward a continual replenishment of its insulin stores (3, 5).

However, there is another contributing factor to consider in control of the β-cell's insulin stores. Normally, a β-cell contains a relatively constant number of β-granules (2, 6), but these are continually turned over, having an estimated half-life of 3–5 d (6, 7). Older β-granules in the β-cell's storage pool that do not

First Published Online June 19, 2007

Abbreviations: ATG, Autophagic gene; 3D, three dimensions/three-dimensional; EM, electron microscope/microscopy; GAPDH, glyceraldehyde-3-phosphate dehydrogenase; GLP-1, glucagon-like peptide-1; KRB, Krebs-Ringer buffer; LAMP, lysosomal-associated membrane protein; PI3Kp85, p85 regulatory subunit of phosphatidylinositol-3′-kinase.

***Molecular Endocrinology* is published monthly by The Endocrine Society (http://www.endo-society.org), the foremost professional society serving the endocrine community.**

undergo exocytosis are eventually retired by intracellular degradation. This intracellular digestion of insulin can be attributed to two mechanisms. The first mechanism is referred to as crinophagy, whereby a β-granule can fuse directly with a large lysosomal-related vacuolar compartment (often referred to as a "crinophagic body") resulting in degradation of the β-granule lumenal content (7–10). The second mechanism is autophagy, which can be subdivided into macroautophagy and microautophagy in terms of degradation of whole organelles (11–13). Macroautophagy is regarded as the primary autophagic mechanism for intracellular protein degradation in mammalian cells (13, 14). In terms of insulin granule degradation, macroautophagy would involve the formation of a membrane around a β-granule to form a double membrane structure termed an "autophagosome." The β-granule-containing autophagosome subsequently docks with a lysosomal vacuole, and their outer membranes fuse to deliver the entire β-granule into the vacuole interior for degradation (13–16). Microautophagy refers to the process whereby a whole β-granule is taken up into a lysosomal compartment by phagocytotic-like mechanism (13, 16). Although both crinophagy and autophagy have been presumed to occur in pancreatic β-cells (7–10), the relative contributions of macroautophagy and/or microautophagy in endocrine cell hormone degradation have not been documented.

Historically, crinophagy has been regarded as the prevalent mechanism for regulating intracellular insulin content in the β-cells of the endocrine pancreas under both normal and abnormal conditions. A crinophagic body in the β-cell contains numerous insulin crystals (1, 6, 8). The insulin crystal is notoriously difficult and slow to degrade by lysosomal proteases (17), explaining why insulin, but not the more soluble C peptide, is detectable in these degradative structures (8). In this study we find that autophagy, as well as crinophagy, significantly contributes to the intracellular β-granule degradation process in β-cells. It is noted that both autophagy and crinophagy use similar large lysosomal-related vacuolar compartments for β-granule/insulin degradation, and as such the term "crinophagic body" to describe these degradation organelles is unfitting. In this text we shall refer to a "multigranular body," as an alternative to a crinophagic body.

The details behind the mechanisms that control intracellular hormone degradation in endocrine cells remain poorly understood (7–9, 18). However, for pancreatic β-cells this is clearly a regulated process. Under conditions where there is little demand for insulin secretion, there is an increase in the intracellular degradation of insulin (6, 7). Conversely, when the rate of insulin secretion is high, there is a corresponding decrease in the rate of insulin degradation within the β-cell (6, 10, 19–21). Thus, the intracellular digestion of insulin granule contents serves as a longer-term regulatory mechanism for keeping insulin content at optimal levels while maintaining the β-cell's capacity to secrete (7, 22).

In this study, we have examined a glucose-intolerant, insulin secretion-deficient animal model, the Rab3A$^{-/-}$ null mouse. Rab3A is a low molecular weight GTP-binding protein that has been shown to direct vesicular traffic in neuroendocrine cells (23). In the β-cell, Rab3A resides on the β-granule membrane, where it plays a role in directing transport of β-granules to the cell surface for subsequent exocytosis (24). In pancreatic islets isolated from Rab3A$^{-/-}$ mice, β-cells secrete approximately 70% less insulin compared with wild-type animals in response to secretagogue stimulation (26). Despite this net overproduction of insulin, insulin content does not markedly increase in Rab3A$^{-/-}$ mouse islets. Here we provide evidence that excessive insulin production, in this instance, is compensated for by a marked increase in insulin degradation facilitated by both autophagic and crinophagic β-granule degradation. Thus, regulating the intracellular digestion of β-granules is a key mechanism for maintaining insulin stores at constant levels in the face of insulin secretory dysfunction in the β-cell. This, in turn, may have consequences for understanding the β-cell's management of intracellular hormone content in other settings of insulin secretory dysfunction, such as type 2 diabetes.

RESULTS

Control of Proinsulin Biosynthesis Is Normal in Rab3A$^{-/-}$ Mouse Islet β-Cells

Preproinsulin mRNA levels in islets isolated from Rab3A$^{-/-}$ and Rab3A$^{+/+}$ animals were comparable after a short (1 h) incubation in the presence of stimulatory (16.7 mM) glucose and did not change compared with levels measured in the presence of basal (2.8 mM) glucose (Fig. 1A). After chronic (18 h) exposure to 16.7 mM glucose, there was a similar 2-fold increase in preproinsulin mRNA levels in both Rab3A$^{-/-}$ and Rab3A$^{+/+}$ islets compared with levels observed at 2.8 mM glucose (Fig. 1A). This reflected a specific glucose-induced increase in preproinsulin mRNA levels, because control glyceraldehyde-3-phosphate dehydrogenase (GAPDH) mRNA levels did not change. In contrast to preproinsulin mRNA levels, there was a specific 4- to 5-fold increase in proinsulin biosynthesis after the 1 h incubation at 16.7 mM glucose compared with that at basal 2.8 mM glucose ($P \leq 0.01$) (Fig. 1B). This rapid, glucose-induced increase in proinsulin biosynthesis above that of general protein synthesis observed in both Rab3A$^{-/-}$ and Rab3A$^{+/+}$ islets, in the absence of any change in preproinsulin mRNA levels, underlines the specific translational control of proinsulin biosynthesis by glucose (3, 4).

Glucose-induced proinsulin biosynthesis after the 18-h incubation at 16.7 mM was 7- to 8-fold higher than that observed at basal 2.8 mM glucose ($P \leq 0.01$) in both Rab3A$^{-/-}$ and Rab3A$^{+/+}$ mouse islets (Fig. 1B). Thus, the approximate 2-fold increase in the mag-

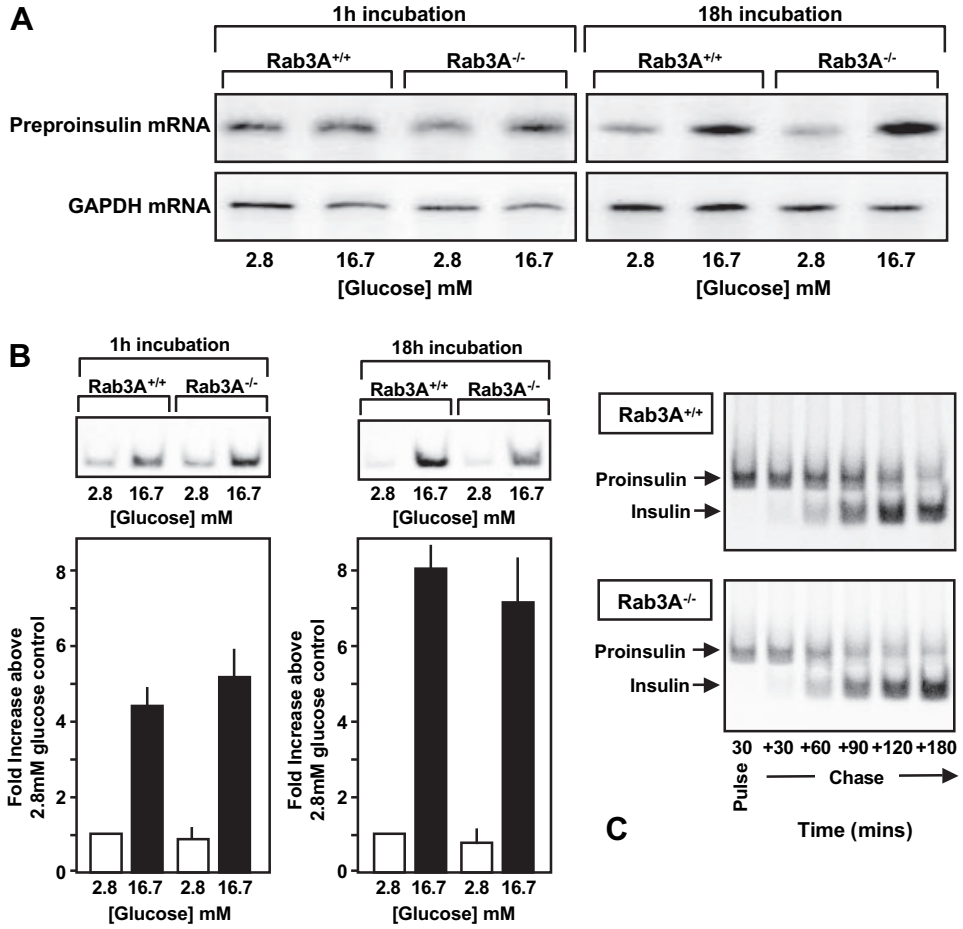

Fig. 1. Proinsulin Biosynthesis Is Normal in Rab3A Mouse Islet β-Cells

Islets isolated from either Rab3A$^{+/+}$ control or Rab3A$^{-/-}$ mice and incubated for either 1 h or 18 h in the presence of basal 2.8 mM or stimulatory 16.7 mM glucose were assessed for preproinsulin mRNA expression and proinsulin biosynthesis as described in *Materials and Methods*. Panel A shows a representative RNase protection assay analysis for preproinsulin and GAPDH (control) mRNA levels. Panel B shows a quantitative analysis of specific proinsulin biosynthesis. Results are expressed as a mean ± SE ($n \geq 4$), expressed as a fold-increase above that measured at basal (2.8 mM) glucose. Representative alkaline-urea gel fluorography analyses for proinsulin biosynthesis are also shown. Panel C shows a representative alkaline-urea gel fluorography analysis of proinsulin to insulin conversion from a pulse-chase radiolabeling experiment in Rab3A$^{+/+}$ and Rab3A$^{-/-}$ mouse islets (as described in *Materials and Methods*), with the electrophoretic migration of proinsulin and insulin indicated.

nitude of glucose-induced proinsulin biosynthesis after an 18-h exposure to stimulatory (16.7 mM) glucose over that observed after a 1-h incubation (Fig. 1B) in both Rab3A$^{-/-}$ and Rab3A$^{+/+}$ islets reflects the specific glucose-induced increase in preproinsulin mRNA levels (Fig. 1A), as previously indicated (4). Taken together, these results demonstrate that mechanisms that control proinsulin biosynthesis, at both the translational and transcriptional levels, remain normal in the Rab3A$^{-/-}$ mouse islet β-cell.

Proinsulin Processing to Insulin Is Normal in Rab3A$^{-/-}$ Mouse Islet β-Cells

Another important mechanism affecting insulin production in the pancreatic islet β-cell is the efficient conversion of proinsulin to insulin and C peptide by limited proteolysis (3). Short-term pulse-chase radiolabeling studies revealed that normal proinsulin conversion in Rab3A$^{-/-}$ mouse islets was indistinguishable from that in control Rab3A$^{+/+}$ mouse islets, with more than 90% of proinsulin converted to insulin within 3 h after initiating proinsulin biosynthesis (Fig. 1C) (25).

Secretagogue-Stimulated Insulin Secretion Is Deficient in Isolated Rab3A$^{-/-}$ Mouse Islets

Glucose-regulated insulin secretion is significantly deficient in Rab3A$^{-/-}$ islet β-cells (26). Here, we examined whether potentiation of glucose-induced insulin secretion by the incretin, glucagon-like peptide 1 (GLP-1), was also diminished in Rab3A$^{-/-}$ islets. A typical sigmoidal response curve for glucose-stimulated insulin secretion for control Rab3A$^{+/+}$ islets was observed, with a threshold at 5–6 mM that reached a

maximal rate at 12–16 mM glucose (Fig. 2A). The addition of GLP-1 significantly potentiated glucose-induced insulin secretion between 8 and 16 mM glucose in normal Rab3A$^{+/+}$ islets (Fig. 2A), as expected (27). In contrast, glucose-stimulated insulin secretion from isolated Rab3A$^{-/-}$ islets was significantly decreased (~70%) compared with control islets (Fig. 2A; $P \leq 0.05$). Moreover, GLP-1-mediated potentiation of glucose-induced insulin secretion was absent in Rab3A$^{-/-}$ islets (Fig. 2A; $P \leq 0.02$), further indicating that the functional secretory capacity of Rab3A$^{-/-}$ islet β-cells was severely restricted (26). It should be noted that this lack of GLP-1-potentiation of glucose-induced insulin secretion was not due to Rab3A$^{-/-}$ islets being unresponsive to GLP-1. GLP-1-stimulated activation of protein kinase-A, as judged by increased phosphorylation of the transcription factor cAMP responsive element binding protein, was still apparent in Rab3A$^{-/-}$ islets and equivalent to that in Rab3A$^{+/+}$ islets (data not shown). The insufficient insulin-secretory response to glucose/GLP-1 in Rab3A$^{-/-}$ islets was more likely reflective of deficient β-granule transport in Rab3A$^{-/-}$ β-cells (24, 26).

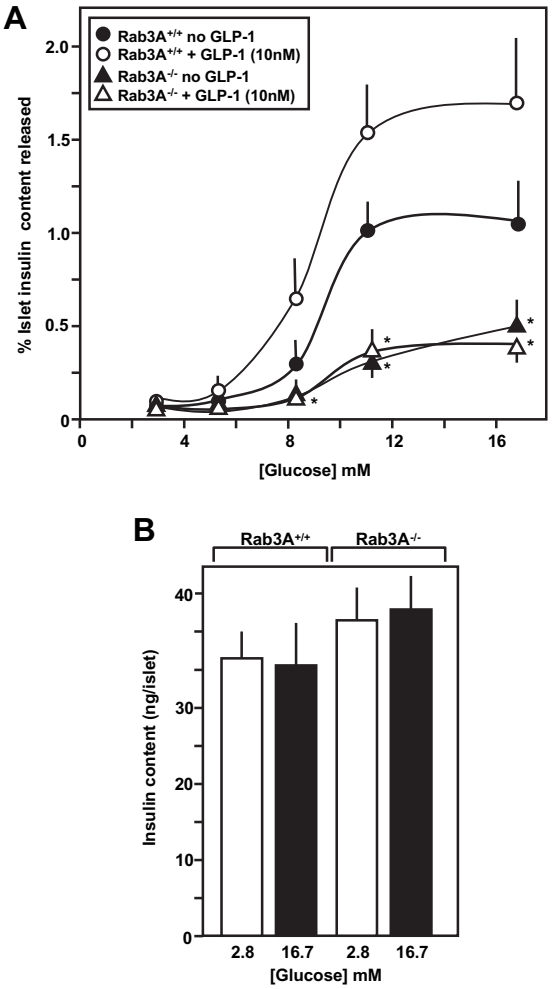

Fig. 2. Secretagogue-Stimulated Insulin Secretion Is Deficient in Isolated Rab3A$^{-/-}$ Mouse Islets

Pancreatic islets were isolated from either Rab3A$^{+/+}$ control or Rab3A$^{-/-}$ mice, incubated for 1 h between 2.8 mM and 16.7 mM glucose ± GLP-1 (10 nM) as indicated, and then assessed for insulin secretion and insulin content as described in *Materials and Methods*. Panel A shows glucose/GLP-1-induced insulin secretion from Rab3A$^{+/+}$ and Rab3A$^{-/-}$ mouse islets where the data are expressed as a mean ± SE ($n \geq 4$) as a fractional release of the islet insulin content, where * indicates significant difference of Rab3A$^{-/-}$ islets from equivalently treated Rab3A$^{+/+}$ control islets ($P \leq 0.05$). Panel B shows the total insulin content of Rab3A$^{+/+}$ and Rab3A$^{-/-}$ mouse islets incubated for 1 h at either a basal (2.8 mM) or stimulatory (16.7 mM) glucose concentration as a mean ± SE ($n = 5$).

Intriguingly, however, despite normal insulin production (Fig. 1), yet defective insulin secretion (Fig. 2A) (26), the insulin content of Rab3A$^{-/-}$ islets was not significantly different from that of control Rab3A$^{+/+}$ islets (Fig. 2B).

Intracellular Insulin Degradation Is Enhanced in Rab3A$^{-/-}$ Islets

An indication of insulin degradation activity in Rab3A$^{-/-}$ and control islets was examined by a longer-term pulse-chase radiolabeling strategy. A window of [^{35}S]protein/[^{35}S](pro)insulin synthesized in a 90-min pulse radiolabeling period was chased in the islets for up to 96 h in culture. The chase period was conducted at a basal 2.8 mM glucose to keep (pro)insulin secretion to a minimum and retain the majority of the [^{35}S](pro)insulin intracellularly (25). Indeed, negligible [^{35}S](pro)insulin was detected in the media of these experiments (data not shown). As such, any difference between detectable [^{35}S](pro)insulin in Rab3A$^{+/+}$ and Rab3A$^{-/-}$islets was most likely reflective of intracellular insulin degradation activity (7).

Total protein degradation in Rab3A$^{+/+}$ and Rab3A$^{-/-}$ islets was similar, with approximate general protein half-lives of 29.6 ± 2.4 h and 32.1 ± 4.2 h, respectively (Fig. 3A). In comparison, [^{35}S](pro)insulin degradation was significantly longer, with an estimated half-life in excess of 3 d (Fig. 3B). This finding is consistent with previous observations of an estimated 3- to 5-d half-life of a β-granule (6, 7), and that the insulin crystal contained in mature β-granules is relatively resistant to lysosomal protease degradation (6, 17). The rate of insulin breakdown in Rab3A$^{-/-}$ islets was observed to be slightly faster than that of Rab3A$^{+/+}$ islets by this pulse-chase radiolabeling analysis at more than 48 h (Fig. 3B). The residual [^{35}S](pro)insulin in Rab3A$^{-/-}$ islets was significantly lower than that in Rab3A$^{+/+}$ control islets at 96 h ($P < 0.05$; Fig. 3B), indicative of increased intracellular insulin degradation activity.

However, we also used a morphological approach to assess intracellular insulin breakdown. Islet β-cells can be readily distinguished from the non-β-cell types by electron microscopy (EM) due to the typical morphological characteristics of β-granules, *i.e*. a small,

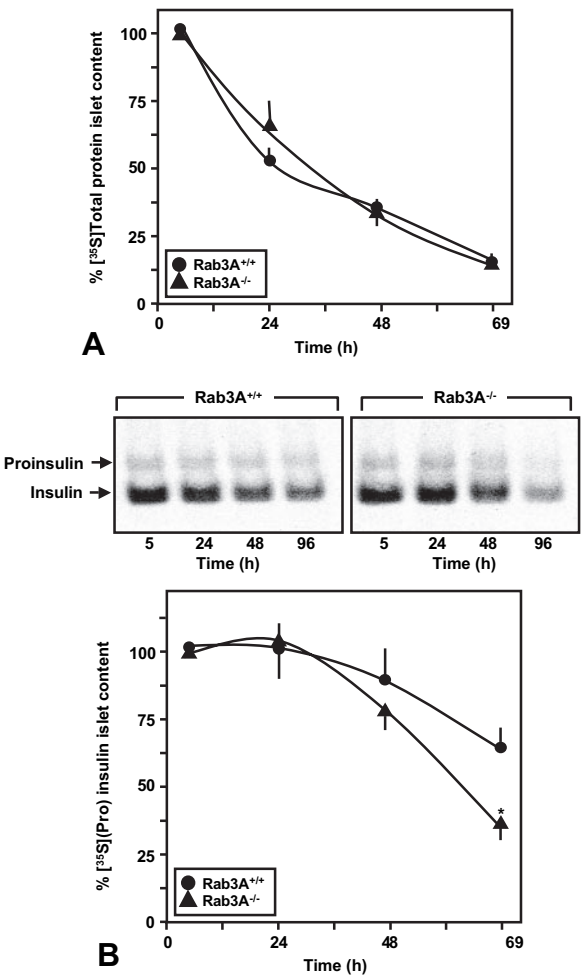

Fig. 3. Intracellular Insulin Degradation Activity Is Enhanced in Rab3A$^{-/-}$ Islets

Pancreatic islets were isolated from either Rab3A$^{+/+}$ control or Rab3A$^{-/-}$ mice and then incubated in a long-term pulse-chase radiolabeling protocol at basal (2.8 mM) glucose for up to 96 h to assess the rate of intracellular total protein and (pro)insulin degradation as described in *Materials and Methods*. Panel A shows the quantitative analysis of residual [^{35}S]total protein present in the Rab3A$^{+/+}$ or Rab3A$^{-/-}$ mouse islets, as indicated, over time relative to "time zero" as a mean ± SE (n ≥ 3), where * indicates significant difference of Rab3A$^{-/-}$ islets from equivalently chased Rab3A$^{+/+}$ control islets ($P \leq 0.05$). Panel B shows the quantitative analysis of residual [^{35}S](pro)insulin present in the Rab3A$^{+/+}$ or Rab3A$^{-/-}$ mouse islets, as indicated, over time relative to "time zero" as a mean ± SE (n ≥ 3). Representative alkaline-urea gel fluorography analyses for [^{35}S](pro)insulin are also shown, with the electrophoretic migration of proinsulin and insulin indicated.

electron-dense core [often hexagonal or rhomboidal in shape as a consequence of insulin crystal structure (28)] surrounded by a large halo (Fig. 4A) (29). Secretory granules in islet non-β-cells have larger, more rounded, dense cores with negligible haloes (Fig. 4B) (30). In the present study, EM analysis revealed that degradative compartments, referred to here as "multigranular bodies," were much more numerous in Rab3A$^{-/-}$ mouse islet β-cells than in Rab3A$^{+/+}$ control mouse islet β-cells (Fig. 4A). It is noteworthy that multigranular bodies were also more numerous in the non-β-cells of Rab3A$^{-/-}$ mouse islet compared with Rab3A$^{+/+}$ mouse islet non-β-cells (Fig. 4B). This is not surprising, given that this animal model represents a total knockout of the Rab3A gene in all tissues (26).

EM Quantification Reveals Increased Intracellular Insulin Degradation in Rab3A$^{-/-}$ Islets

EM analyses were carried out on three separate islet preparations from Rab3A$^{-/-}$ and Rab3A$^{+/+}$ mice, utilizing three to five separate blocks (containing two to five embedded islets per block) per islet preparation. Quantification was based on counting multigranular bodies in selected 5-μm^2 surface areas of individual islet cells (excluding the nucleus) in the electron micrograph sections. A total of 482 5-μm^2 areas from a total of 347 β-cells from control Rab3A$^{+/+}$ mouse islets; 456 5-μm^2 areas from 309 β-cells of Rab3A$^{-/-}$ mouse islets; 92 5-μm^2 areas from 63 non-β-cells of control Rab3A$^{+/+}$ mouse islets; and 80 5-μm^2 areas from 57 non-β-cells of Rab3A$^{-/-}$ mouse islets were counted. Because non-β-cells are less frequent in rodent pancreatic islets, and it is more difficult to distinguish between the α-, δ-, pp-, and ε-cells at the EM level by granule morphology alone, non-β-cell data were grouped together into a single category. A large number of 5-μm^2 surface areas in islet cell electron micrographs were counted to minimize sectioning artifacts.

On average, control Rab3A$^{+/+}$ islets contained 0.36 ± 0.04 multigranular bodies/5-μm^2 β-cell section surface area. In contrast, Rab3A$^{-/-}$ mouse islet β-cells contained significantly more 4.41 ± 0.20 multigranular bodies/5-μm^2 β-cell section surface area, implicating a 12.3-fold increase relative to control mice ($P \leq 0.001$; Fig. 5A). Moreover, multigranular bodies were found to be significantly larger in Rab3A$^{-/-}$ *vs.* Rab3A$^{+/+}$ islet β-cells (analysis of 1522 and 233 multigranular bodies, respectively; $P \leq 0.001$; Fig. 5A), and contained more residual insulin crystals ($P \leq 0.001$; Fig. 5A) compared with control animals. Thus, intracellular insulin degradative activity was higher in Rab3A$^{-/-}$ *vs.* Rab3A$^{+/+}$ mice.

Increased lysosomal digestion of intracellular hormone content was not confined to pancreatic β-cells in the Rab3A$^{-/-}$ mouse model. Although multigranular bodies were not as abundant in other islet endocrine cell types compared with islet β-cells (on average, one multigranular body was seen for every four non-β-cells, quantified as 0.24 ± 0.02 multigranular bodies/5-μm^2 non-β-cell section surface area; Fig. 5B), Rab3A$^{-/-}$ mouse islet non-β-cells revealed a significant 8.7-fold increase in the number of degradative compartments relative to control animals at 2.08 ± 0.22 multigranular bodies/5-μm^2 non-β-cell section surface area ($P \leq 0.001$; Fig. 5B). In contrast to β-cells,

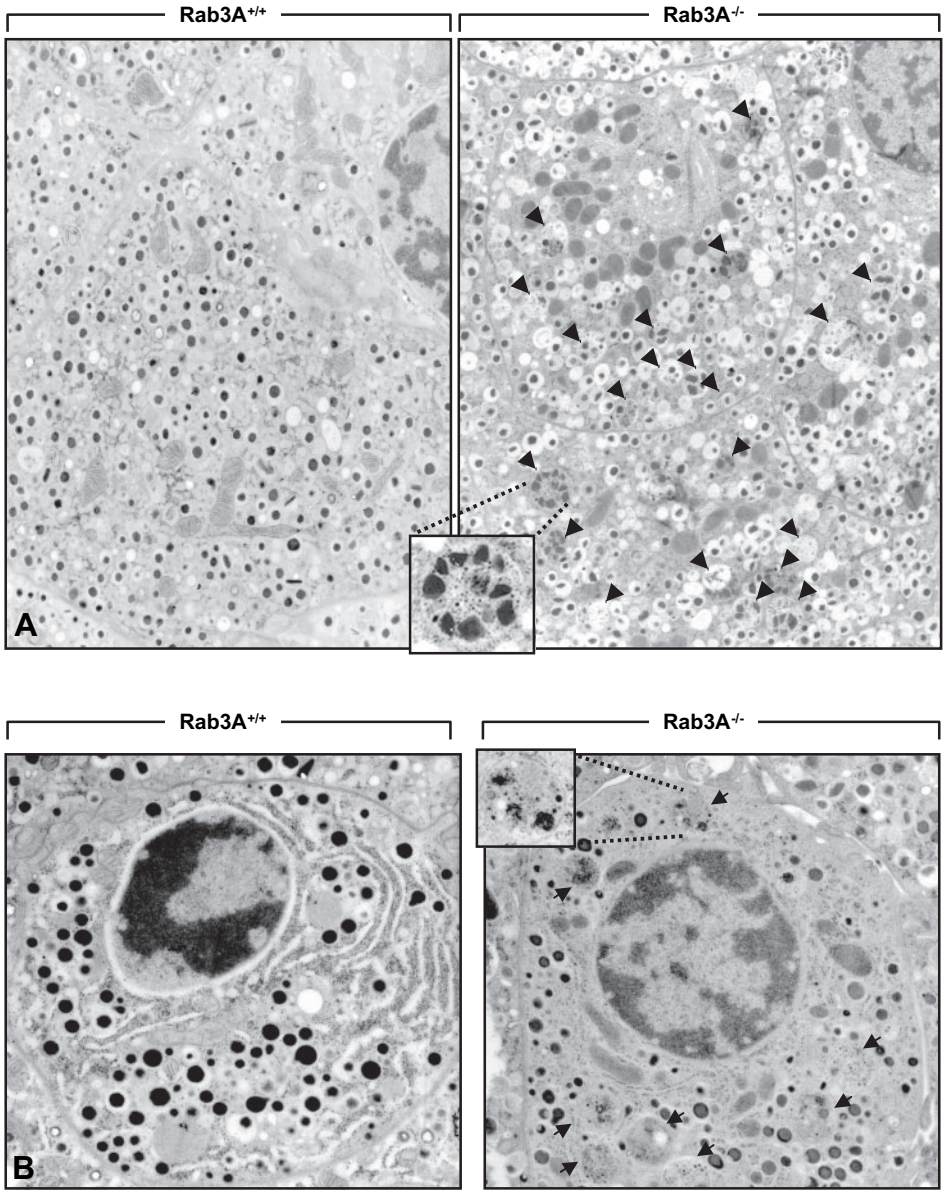

Fig. 4. Intracellular Degradation in Rab3A$^{-/-}$ Islet Cells Is Increased Compared with Control Rab3A$^{+/+}$ Islet Cells as Assessed by Conventional EM Analysis

Pancreatic islets were isolated from Rab3A$^{+/+}$ control and Rab3A$^{-/-}$ mice and surveyed by conventional EM as described in *Materials and Methods*. Panel A shows a representative image of Rab3A$^{+/+}$ and Rab3A$^{-/-}$ mouse islet β-cells (magnification, $\times$6600). Multigranular bodies occurred at low frequency in Rab3A$^{+/+}$ β-cells, but were numerous in Rab3A$^{-/-}$ β-cells (*arrowheads*). An example multigranular body from a β-cell is magnified further in the *inset*. Panel B shows a representative images of Rab3A$^{+/+}$ and Rab3A$^{-/-}$ mouse islet non-β-cells (magnification, $\times$6600). As with β-cells, multigranular bodies were rarely observed in other pancreatic islet endocrine cell types of Rab3A$^{+/+}$ mice, yet were numerous in the same cell types in Rab3A$^{-/-}$ mice (*arrowheads*). A representative multigranular body from an islet non-β-cell is magnified in the *inset*.

the average size of multigranular bodies did not differ between control and Rab3A$^{-/-}$ mice (Fig. 5B). Residual secretory granule cores were not consistently observed in non-β-cell multigranular bodies and thus could not be quantified, presumably due to the fact that their primary hormone products (*i.e*. glucagon, somatostatin, pancreatic polypeptide, and ghrelin in α-, δ-, pp-, and ε-cells, respectively) are more soluble and thus more readily degraded than the paracrystalline insulin core within mature β-granules (17).

Although two-dimensional EM surveys of thin sections indicated increased degradation of β-granules/insulin in Rab3A$^{-/-}$ islet β-cells mediated by an apparent 12-fold increase in the number of multigranular bodies per β-cell surface area (Fig. 5), we wanted to rule out the possibility that this increase was due to the

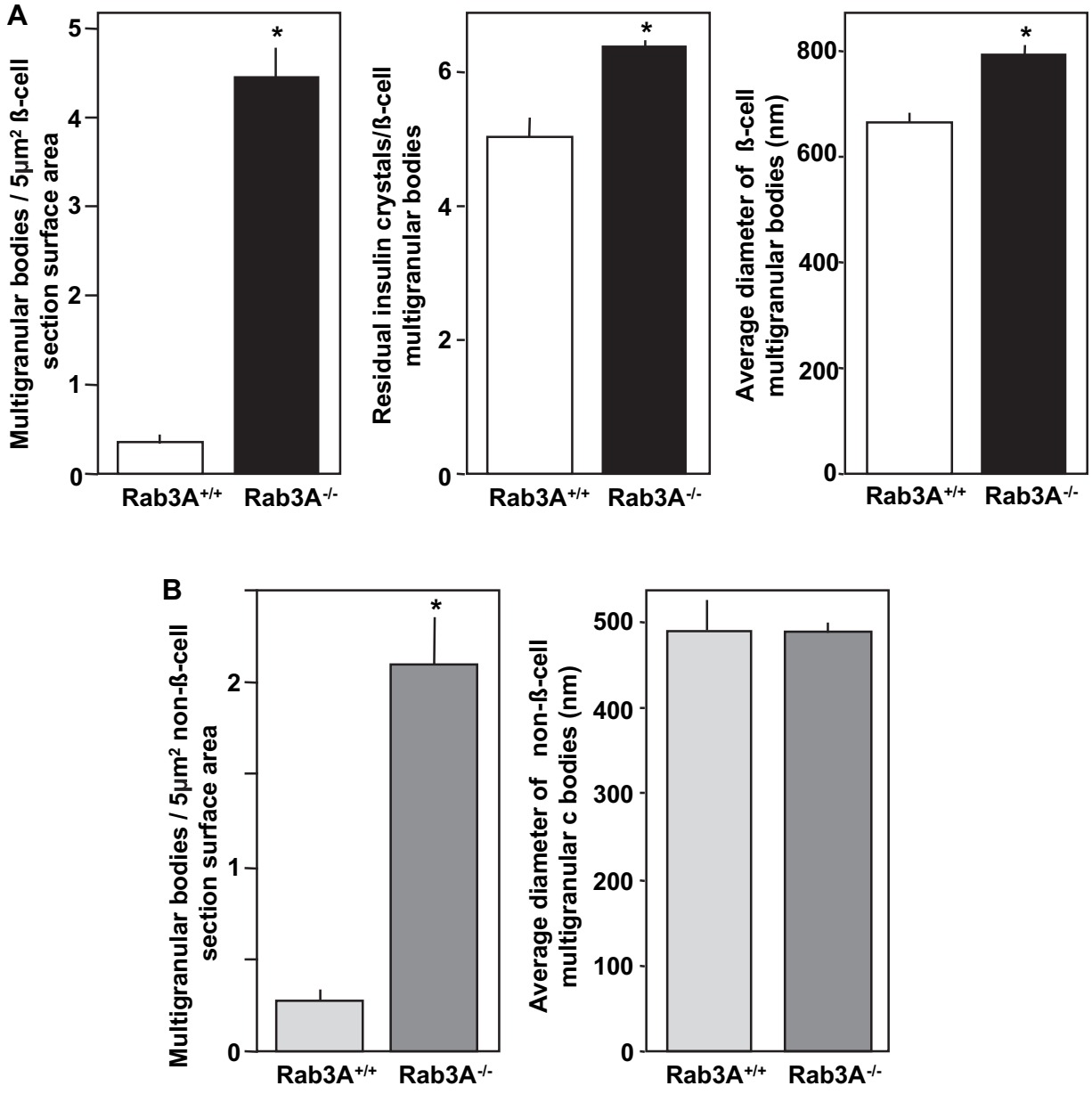

Fig. 5. Multigranular Bodies Are Larger and More Numerous in Rab3A$^{-/-}$ Islet β-Cells

Pancreatic islets were isolated from Rab3A$^{+/+}$ control and Rab3A$^{-/-}$ mice and then analyzed by conventional two dimensional EM as described in *Materials and Methods*. In panel A, a quantification of multigranular bodies per 5-μm^2 surface area regions of islet β-cells from Rab3A$^{+/+}$ (n = 482 5-μm^2 regions from 347 β-cells) and Rab3A$^{-/-}$ (n = 456 5-μm^2 regions from 309 β-cells) mouse islets is presented, including the number of multigranular bodies per β-cell, the number of residual insulin crystals per multigranular body, and the average diameter of a β-cell multigranular body. Data are shown as mean ± SE. In Panel B, a quantification of multigranular bodies per 5-μm^2 surface area regions in islet non-β-cells from Rab3A$^{+/+}$ (n = 92 5-μm^2 regions from 63 non-β-cells) and Rab3A$^{-/-}$ (n = 80 5-μm^2 regions from 57 non-β-cells) mouse islets is likewise presented (mean ± SE). In all panels the * indicates significant difference of Rab3A$^{-/-}$ islets from Rab3A$^{+/+}$ control islets ($P \leq 0.05$).

limitations of conventional EM. For example, some multigranular bodies resided in close proximity to each other, which might have suggested a single larger tubular degradative compartment that had been cut in several places in the plane of view to reveal an apparent increase in the number of individual multigranular bodies. Thus, we analyzed the structure of several multigranular bodies using a three-dimensional (3D) EM technique referred to as electron tomography (ET), to unambiguously address the nature of these compartments at high resolution (~6 nm) and in 3D (31, 32). Representative 3D reconstructions of multigranular bodies in mouse islet β-cells are presented in QuickTime Movies 1–4 (see supplemental data pub-

lished on The Endocrine Society's Journals Online web site at http://mend.endojournals.org). The tomographic analysis indicated that although often multilobed, each multigranular body visible within a plane of section indeed represented a single degradative compartment rather than a portion of a large, continuous tubular system.

The number of β-granules per β-cell surface area (excluding the nucleus) was also examined in the same electron micrographs. In Rab3A$^{+/+}$ control mouse islets, an average of 74.8 ± 2.6 β-granules/5-μm^2 β-cell section surface area was observed, whereas in Rab3A$^{-/-}$ mouse islets a significantly less 52.8 ± 1.8 β-granules/5-μm^2 β-cell section surface area was found ($P \leq 0.001$). This represents a 29.4% decrease in β-granules in Rab3A$^{-/-}$ *vs.* Rab3A$^{+/+}$ control mouse islets. It should be noted that this β-granule decrease is not reflected in the islet insulin content of Rab3A$^{-/-}$ mouse islets (Fig. 2B), because this is also contributed by the residual insulin crystals found in the increased numbers of multigranular bodies in Rab3A$^{-/-}$ mouse islet β-cells (Fig. 5). Moreover, considering that islet β-cells secrete only 1–2% of their intracellular insulin stores per hour under stimulatory conditions (Fig. 2A), it is unlikely that this approximately 30% decrease in β-granules in Rab3A$^{-/-}$ mouse islet β-cells impinges on insulin-secretory capacity.

EM Evidence of Increased β-Granule Crinophagy and Autophagy in Rab3A$^{-/-}$ Islets

The intracellular degradation of insulin and turnover of β-granules in β-cells is presumed to be facilitated by both crinophagy and autophagy (6, 10). However, these processes have not been clearly demonstrated to occur simultaneously in pancreatic β-cells. Because of the high incidence of β-granule/insulin degradation in Rab3A$^{-/-}$ mouse islet β-cells, we were able to capture examples of crinophagy in which β-granules were apparently docked with multigranular bodies (Fig. 6A). An area of *darkened shading* on the electron micrographs at the point of contact between the β-granule and multigranular body membranes (as indicated by the *arrow* on Fig. 6A), suggested that these organelles were indeed in physical contact. In addition, rare images of β-granules already fused with multigranular bodies were acquired (Fig. 6, B and C), with their membranes continuous in some cases (Fig. 6C), indicating that the process of crinophagy had occurred.

We have also found that autophagy significantly contributes to β-granule/insulin degradation in Rab3A$^{-/-}$ mouse islet β-cells. Rare EM evidence of both macroautophagy and microautophagy in these β-cells was obtained. The early stages of macroautophagy were observed, where membranes gathered around a β-granule (Fig. 6D) to form a double-membraned vesicle encapsulating an entire β-granule (Fig. 6E); this early organization of autophagic membranes is known as an "autophagosome" (13, 14). The docking of autophagosomes to multigranular bodies to facilitate the delivery of β-granules *in toto* into degradative compartments was also frequently observed (Fig. 6F). This process results in digestion/breakdown of the β-granule membrane inside the multigranular body, as well as the granule's luminal contents such as insulin (Fig. 6G). Furthermore, it was also possible to capture images of the process of microautophagy, whereby degradative/multigranular structures selectively phagocytose and engulf entire β-granules (Fig. 6, H–J). This process, like macroautophagy yet in contrast to crinophagy, results in the degradation of the β-granule membrane in addition to the granule cargo (Fig. 6K), but in a selective rather than bulk autophagic manner.

Tomographic analyses of the 3D organization of β-cell organelles revealed that the majority of multigranular bodies in Rab3A$^{-/-}$ mouse islet β-cells have invaginations, indicative of microautophagic activity. A Quicktime movie (supplemental Movie 5) shows a multigranular body with invaginations revealed to be continuous with the cytosol by EM-tomography, clearly indicating its microautophagic activity. A 3D surface-rendered model generated by segmentation of the tomographic reconstruction of this particular multigranular body highlights such invaginations and microautophagic uptake (supplemental Movie 6).

Examination of Autophagic Gene (ATG) Expression in Rab3A$^{-/-}$ *vs.* Rab3A$^{+/+}$ Isolated Mouse Islets

A family of genes (known as ATGs) has been implicated in the control of macroautophagy (12, 14, 16, 33). However, it essentially remains unclear how crinophagy and microautophagy are differentially regulated (16). Nonetheless, we examined whether there was an alteration in the expression of key ATGs in isolated islets of Rab3A$^{+/+}$ *vs.* Rab3A$^{-/-}$ mice by semiquantitative RT-PCR analysis using β-actin mRNA expression as a reference that did not alter between Rab3A$^{+/+}$ *vs.* Rab3A$^{-/-}$ mouse islets (Fig. 7A). As observed previously (Fig. 1), there was no change in preproinsulin gene expression between Rab3A$^{+/+}$ *vs.* Rab3A$^{-/-}$ mouse β-cells (Fig. 7A). For most of the ATGs examined there was no significant difference in their expression between islets from Rab3A$^{+/+}$ *vs.* Rab3A$^{-/-}$ mice (Fig. 7, A and B). There was a trend for ATG5 to be slightly increased in Rab3A$^{-/-}$ mouse islets, but this was not statistically significant (Fig. 7, A and B). Likewise, there was no change in the expression of the lysosomal protein, LAMP-1 (Fig. 7, A and B). However, in contrast, there was a specific 67% significant decrease in the related LAMP-2 gene expression ($P < 0.01$; Fig. 7, A and B). Although a semiquantitative RT-PCR approach can reveal large qualitative changes in mRNA expression levels, it is not necessarily a reliable quantitative method. As such, the expression levels of LAMP-1 and

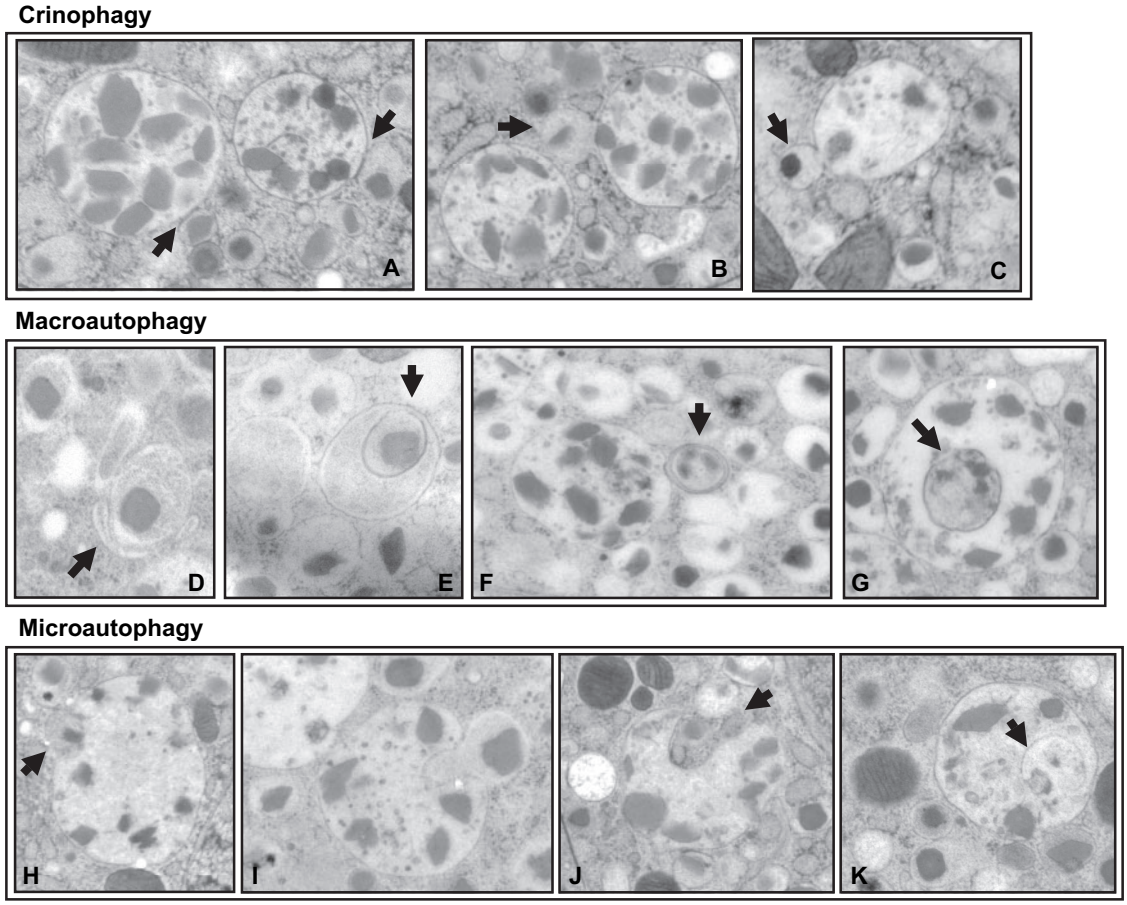

Fig. 6. Morphological Evidence for the Up-Regulation of Crinophagy, Macroautophagy, and Microautophagy in Rab3A$^{-/-}$ Islet β-Cells

Pancreatic islets were isolated from Rab3A$^{-/-}$ mice and then analyzed by conventional EM as described in *Materials and Methods*. As β-granule/insulin degradation activity was dramatically increased in Rab3A$^{-/-}$ islet β-cells, numerous examples of crinophagy were observed. Panels A–C reveal different stages of β-granule crinophagy. Panel A shows a granule docked against a multigranular body, whereas panels B and C show instances of the β-granule membrane fusing with that of the multigranular body (*arrowheads*). Example images showing the process of macroautophagy are shown in the *upper* set of panels (D–G). Panel D shows an early stage of macroautophagy where membranes are gathering around a β-granule (*arrowheads*). Panel E shows a β-granule captured inside an autophagosome, as indicated by the *arrowhead*. Panel F shows an autophagosome docked with a multigranular body (*arrowhead*) to deliver a β-granule to its degradative interior. Panel G shows a β-granule inside a multigranular body with the β-granule membrane intact (*arrowhead*), indicating that autophagosome-mediated delivery of a β-granule to the degradative compartment had occurred. Panels H and I show microautophagy, whereby a multigranular body is engulfing an entire β-granule by phagocytosis. Panel K shows a β-granule inside a multigranular body with the β-granule membrane mostly intact (*arrowhead*).

LAMP-2 in Rab3A$^{+/+}$ *vs.* Rab3A$^{-/-}$ mouse isolated islets were reexamined by fluorescence-based real-time quantitative RT-PCR, following a method previously described using β-actin mRNA levels as a reference (34). This more quantitative approach also indicated that expression levels of LAMP-1 were unchanged, but there was a significant approximately 80% decrease in LAMP-2 mRNA levels in Rab3A$^{+/+}$ *vs.* Rab3A$^{-/-}$ mouse isolated islets ($P \leq 0.05$; Fig. 5C).

This decrease in LAMP-2 gene expression was also reflected at the protein level, where LAMP-2 protein in isolated Rab3A$^{-/-}$ mouse islets was reduced approximately 80% compared with Rab3A$^{+/+}$ mouse islets ($P \leq 0.05$; Fig. 7D). LAMP-1 protein expression and that of the p85 regulatory subunit of phosphatidylinositol-3′-kinase (PI3Kp85; used as a loading control) did not change between Rab3A$^{+/+}$ *vs.* Rab3A$^{-/-}$ mouse islets (Fig. 7D), emphasizing a specific decrease of LAMP-2 expression in Rab3A$^{-/-}$ mouse islets. It should be noted that LAMP-2 is a negative regulator of autophagy (35, 36), and this reduced expression LAMP-2 in Rab3A$^{-/-}$ mouse islets correlated with the increased autophagy observed.

DISCUSSION

Although the contribution of intracellular degradation to the regulation of cellular insulin content is often

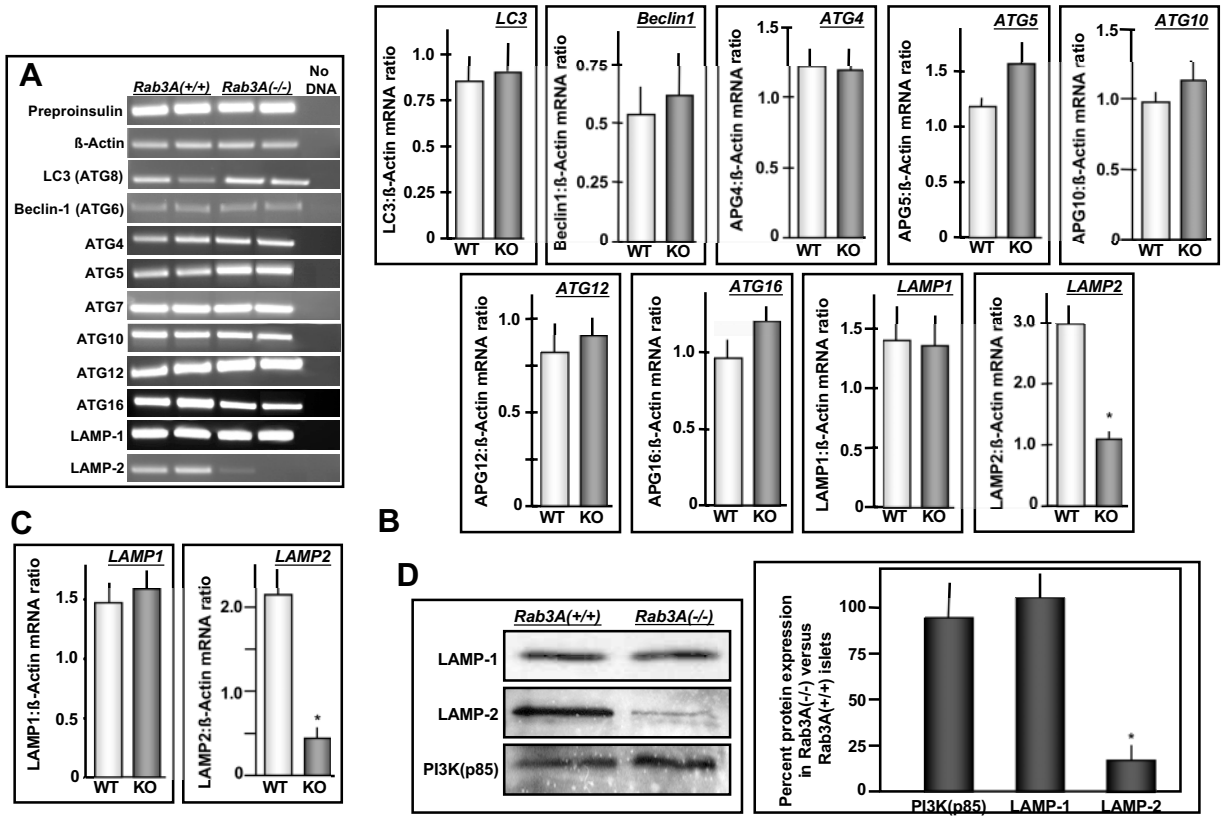

Fig. 7. LAMP-2 Gene Expression Is Specifically Down-Regulated in Rab3A$^{-/-}$ Islet β-Cells

Pancreatic islets were isolated from individual Rab3A$^{+/+}$ and Rab3A$^{-/-}$ mice (20–24 wk of age) and then analyzed for the gene expression of preproinsulin-1 and -2, β-actin (reference control), the macroautophagic genes, ATG4, ATG5, and ATG6 (also known as beclin-1), ATG7 and ATG8 (also known as LC3), ATG10, ATG12, and ATG16, as well as the lysosomal-associated membrane proteins, LAMP-1 and LAMP-2, by semiquantitative RT-PCR as described in *Materials and Methods*. Panel A shows an example RT-PCR analysis of islet preparations from two separate Rab3A$^{+/+}$ and Rab3A$^{-/-}$ mice. Panel B shows the accumulated semiquantitative RT-PCR analysis gene expression in Rab3A$^{+/+}$ *vs.* Rab3A$^{-/-}$ mouse islets relative to β-actin mRNA expression. The data are presented as a mean $\pm$ SE ($n \geq 6$). Panel C shows a quantitative real time RT-PCR analysis of LAMP-1 and LAMP-2 mRNA expression levels relative to β-actin mRNA expression in Rab3A$^{+/+}$ *vs.* Rab3A$^{-/-}$ mouse islets The data are presented as a mean $\pm$ SE ($n \geq 3$). Panel D shows a representative immunoblot analysis (*left panel*) of the specific decreased LAMP-2 protein expression in isolated islets from Rab3A$^{-/-}$ mice relative to Rab3A$^{+/+}$ mouse islets and that of LAMP-1 and PI3Kp85 used as a loading control. The *right panel* shows a quantification of the percentage change in PI3Kp85, LAMP-1, and LAMP-2 protein levels, determined by immunoblot analysis, in Rab3A$^{-/-}$ mice relative to Rab3A$^{+/+}$ mouse islets. These data are presented as a mean $\pm$ SE ($n = 4$). In panels B–D the * indicates significant difference in Rab3A$^{-/-}$ mice relative to Rab3A$^{+/+}$ mouse islets of $P \leq 0.05$. KO, Knockout; WT, wild type.

under appreciated, it nonetheless plays an important role over the long term to cap insulin levels and facilitate normal β-granule turnover (6, 7, 9, 10, 22). In this study, we have revealed a redistribution in the normal balance between insulin production, secretion, and degradation in the β-cell in an animal model of deficient insulin secretion, the Rab3A$^{-/-}$ mouse (26). In the β-cells of islets isolated from these mice, the regulation of insulin gene transcription, proinsulin synthesis at the translational level, and proinsulin processing to insulin are indistinguishable from control Rab3A$^{+/+}$ islet β-cells. Hence insulin production is normal in Rab3A$^{-/-}$ mouse islet β-cells. However, in the absence of Rab3A, defective β-granule transport results in an approximately 70% reduction in secretagogue-induced insulin secretion (26) (Fig. 2). Yet, despite the net overproduction of insulin in Rab3A$^{-/-}$ islet β-cells, intracellular insulin levels were apparently not significantly different from controls due to the marked up-regulation in intracellular insulin/β-granule degradation by autophagy and crinophagy.

Crinophagy has been previously deemed to be the major mechanism of intracellular insulin degradation in the β-cell (6, 8, 10), but this study has revealed a critical role for autophagy in management of β-granule/insulin content *in vivo*, under conditions where insulin secretion is impaired. Previous studies that used diazoxide to inhibit insulin secretion without affecting insulin production reported a significant increase in intracellular insulin content concomitant with increased lysosomal enzyme activity and crinophagy, but not autophagy (9, 10). This increase in insulin

content observed in diazoxide-treated islets reflected that a transient increase in crinophagy alone was insufficient to redress the net oversupply of intracellular insulin. Here, in contrast, we find that in an *in vivo* model of insulin-secretory deficiency, the Rab3A$^{-/-}$ mouse, excess insulin production in β-cells is counterbalanced by a up-regulation of autophagic degradative pathways, as well as crinophagy, to maintain intracellular insulin stores at near-normal levels over the long term. Consistent with other studies, increased intracellular insulin breakdown in Rab3A$^{-/-}$ mouse β-cells was indicated by a marked increase in degradative compartments (7–10, 22). These compartments are historically referred to as "crinophagic bodies" because crinophagy has been documented as the major mechanism of secretory granule degradation in the β-cell (6, 22). Indeed, EM evidence in this study indicated that crinophagy does contribute to increased insulin/β-granule degradation in β-cells of Rab3A$^{-/-}$ islets (Fig. 6). However, autophagy, particularly microautophagy, was also markedly increased in Rab3A$^{-/-}$ islet β-cells compared with Rab3A$^{+/+}$ control β-cells. It is this augmentation in autophagic activity over the long term that likely compensates for the overproduction of insulin in Rab3A$^{-/-}$ islet β-cells *in vivo* to maintain intracellular insulin stores at near-normal levels.

Autophagy is subdivided into different mechanisms, referred to as "macroautophagy," "microautophagy," and "chaperone-mediated autophagy" (13, 14, 16). Both macroautophagy and microautophagy were observed in Rab3A$^{-/-}$ islets (Fig. 6). Chaperone-mediated autophagy is a selective mechanism by which certain cytosolic proteins are delivered to and degraded in lysosomal compartments (16, 37). As such, it is quite unlikely to be involved in the selective degradation of a whole organelle, such as β-granule, as found in Rab3A$^{-/-}$ mouse β-cells. Likewise, proteosomal degradation mechanisms are not involved in intracellular degradation of insulin in β-cells (38). Due to the high levels of β-granule/insulin degradation in Rab3A$^{-/-}$ islet β-cells, multiple stages of macroautophagy were documented, including an autophagosome (Fig. 6, D–F) (13, 14, 16, 39), and, more commonly, microautophagy in which individual β-granules are imbibed into a multigranular degradation compartment by a phagocytotic mechanism (Fig. 6, H–J, and supplemental Movies 5 and 6). These data provide the first evidence that macroautophagy and microautophagy act in concert with crinophagy to regulate β-granule/insulin content in β-cells, under conditions in which regulated secretion is impaired and insulin production is excessive.

There is an important functional implication between crinophagy and autophagy in terms of β-granule degradation in the β-cell. Because crinophagy involves the fusion of the β-granule and multigranular body outer membranes, a β-granule membrane protein is incorporated into the multigranular body membrane and is probably not subject to lysosomal degradation. Presumably, β-granule membrane constituents are recycled back to the Golgi for use in subsequent rounds of insulin granule packaging (40). In contrast, the autophagic mechanisms documented here result in delivery of the entire β-granule to the lumen of the multigranular body/lysosomal compartment (12–14), so that both lumenal cargo and membrane components of the β-granule are proteolytically degraded. As such, autophagy plays a much more prominent role in β-granule turnover than previously thought, particularly under conditions where a marked increase in intracellular degradation is required. Moreover, because the insulin contained in the multigranular bodies will be irreversibly degraded [albeit slowly (17)], it no longer is able to contribute to the β-cell's insulin-secretory capacity. Therefore, measurements of islet total insulin content do not always provide an accurate measurement of β-cell-secretory capacity, where a sizeable proportion of intracellular insulin terminally resides in multigranular body/degradative compartments. Nonetheless, most likely because of increased β-granule autophagic activity in the Rab3A$^{-/-}$ islet β-cells, a 30% reduction in β-granule number was observed. However, it is unlikely that this moderate decrease in β-granules will contribute to insulin-secretory dysfunction in this model. A β-cell's ability to secrete insulin only reflects a minor subpopulation of β-granules that remain capable of readily undergoing exocytosis (2, 41). This is reflected in a 1–2% of the total β-granule population secreted/hour under marked stimulated conditions (Fig. 2A).

The increase of autophagy in Rab3A$^{-/-}$ islet β-cells compensates for the abnormal imbalance between insulin secretion and insulin production. This implies that intracellular insulin degradation activity is a highly regulated process, and that maintenance of insulin stores is an important aspect of β-cell function. A question arises as to what controls the increase in multigranular bodies in Rab3A$^{-/-}$ islet β-cells selective for β-granule degradation. An initial examination of the expression of key genes implicated in multigranular body degradation mechanisms between isolated islets from Rab3A$^{+/+}$ and Rab3A$^{-/-}$ mice indicated that there was no significant difference in the expression of ATGs implicated in the up-regulation of macroautophagy (12, 14, 16, 33). However, increased ATG expression is more associated with a response to starvation or pathogenic infections and directed at the process of aggregating soluble proteins destined for macroautophagic degradation, rather than degradation of whole organelles (33, 42). This suggests that macroautophagy, although present, was not a major contributor to β-granule degradation in Rab3A$^{-/-}$ mouse islet β-cells, consistent with the observation that microautophagy was more common. In contrast to ATGs, the expression of the lysosomal associated membrane protein, LAMP-2, but not that of the related LAMP-1, was significantly decreased in Rab3A$^{-/-}$ *vs.* Rab3A$^{+/+}$ mouse islets (Fig. 7). LAMP-2 has been shown to be a negative regulator of autophagy (35, 36), and disabling mutations in LAMP-2 are associated

with Danon disease in humans (43). In Danon disease and LAMP-2$^{-/-}$ mice there is a marked increase in autophagic vacuoles in many tissues causing cardiomyopathy, myopathy, and neuronal degeneration (33, 35, 42, 44). As such, it is quite possible that the specific decreased expression of LAMP-2 in Rab3A$^{-/-}$ mouse islets causes an increase in multigranular body degradation compartments in β-cells and increased β-granule/insulin degradation. This implies that LAMP-2 might be dynamically regulated in β-cells to control autophagic degradation of organelles, like β-granules. Because no change in ATG expression was observed in Rab3A$^{-/-}$ mouse islets, it is likely that the increased autophagic degradation of β-granules was more commonly contributed by increases in microautophagy and less so by macroautophagy. However, it should also be considered that a multigranular body in the β-cell may originally be derived from a lysosome (20, 21), and thus the significant increase in the number of these degradation compartments in Rab3A$^{-/-}$ mouse islet β-cells implies that the regulation of lysosomal biogenesis will also contribute to controlling insulin/β-granule degradation in the β-cell (45, 46). Because LAMP-2 is a lysosomal-membrane protein, a decrease in its expression may favor formation of mircoautophagic multigranular bodies from lysosomes in β-cells. However, in general, the mechanisms that regulate microautophagy in mammalian regulated secretory cells remain undetermined (16), and further experimentation will be required to determine whether the specific decrease in LAMP-2 expression triggers the up-regulation of (micro)autophagic activity in β-cells.

It is possible that the findings in this study might be peculiar to the Rab3A$^{-/-}$ mouse model. However, it is unlikely that deletion of Rab3A leads to increased β-granule degradation. Of more than 40 members of the Rab family of proteins involved in directional vesicular trafficking, only Rab7 has been implicated in autophagy (47). Considering that an imbalance between insulin production and secretion in β-cells leads to adaptive β-granule degradation under other circumstances (7, 10, 19, 21, 22), we favor this reason as the cause of increased crinophagic and autophagic activity in Rab3A$^{-/-}$ mouse islet β-cells. However, further experimentation is required to substantiate this idea, and for the moment alternative explanations cannot be ruled out.

Notwithstanding, it should be noted that increased autophagy has been associated with the pathogenesis of human type 2 diabetes (48), and our findings here might have relevance. In certain models of type 2 diabetes, both insulin gene expression and proinsulin biosynthesis can be unchanged or even up-regulated in contrast to insulin secretory dysfunction and deficiency in the same β-cell population, acquiring an imbalance between insulin production and secretion reminiscent of the Rab3A$^{-/-}$ mouse β-cell phenotype (26). This implies that β-granule degradation could well be up-regulated in the β-cell during the progression of type 2 diabetes, to counter excessive insulin production. Initially, this may be a protective effect to avert over accumulation of β-granules within the β-cell. Although autophagic β-granule degradation may be initially selective for β-granules, if continued chronically, it could become less discriminatory and other β-cell organelles might be degraded resulting in autophagic mediated-death of β-cells (16, 33), which in turn would contribute to decreased β-cell mass that marks the onset of type 2 diabetes (49). Indeed, there is precedence of this in that chronic autophagic programmed cell death type II (also known as nonapoptotic cell death) has been shown to be a significant contributing factor to certain myopathies and the later stages of neuronal degenerative diseases (16, 33). Although the current study in Rab3A$^{-/-}$ mouse islet β-cells newly reveals the potential of β-cell autophagy as a contributing factor in the pathogenesis of type 2 diabetes, future experiments will be needed to reaffirm its part in either the increased incidence of β-cell death and/or secretory dysfunction that marks the onset/progression of the disease in humans.

MATERIALS AND METHODS

Materials

The EasyTag Expre^{35}S^{35}S Protein Labeling Mix from New England Nuclear (Boston, MA), containing 73% of L-[^{35}S]methionine, was used for islet protein synthesis radiolabeling, referred to as [^{35}S]methionine. Uridine 5′-[α-^{32}P]trisphosphate (3000 Ci/mmol) was purchased from Amersham Pharmacia Biotech, Inc. (Piscataway, NJ). GLP-17–36 was purchased from Bachem, Inc. (King of Prussia, PA). All other reagents were of analytical grade and obtained from either Sigma Chemical Co. (St. Louis, MO) or Fisher Scientific, Inc. (Pittsburgh, PA).

Animals

The Rab3A$^{+/+}$ on a B6 background (B6129SF2/J) and Rab3A$^{-/-}$ mice were obtained from The Jackson Laboratory (Bar Harbor, ME) (26). Mice were housed on a 12-h light, 12-h dark cycle and were allowed free access to standard mouse food and water. Mice were used at 18–24 wk of age. Animal experimentation was conducted in accord with accepted standards of humane animal care as outlined by the National Institutes of Health Guide for the Care and use of Laboratory Animals and approved by the Institutional Animal Use and Care Committees at the University of Chicago.

Islet Isolation and *in Vitro* Insulin Secretion

Pancreatic islets of Langerhans were isolated by collagenase digestion followed by Histopaque-Ficoll density gradient centrifugation as previously described (50). For static incubations, 20–25 freshly isolated islets were preincubated in 500 μl Krebs-Ringer buffer (KRB) containing basal 2.8 mM glucose and 0.1% BSA (wt/vol) for 60 min at 37 C, and then incubated for a further 60 min in the same volume of KRB/0.1% BSA containing basal 2.8 mM glucose, stimulatory 16.7 mM glucose, or 16.7 mM glucose ± 1 nM GLP-1. After this second incubation at 37 C, the media were removed and the islets placed in 200 μl lysis buffer (50 mM HEPES, pH 7.5; 1%

Nonidet P-40; 2 mM Na vanadate; 100 mM NaF; 4 mM EDTA; 1 μM leupeptin; 10 μg/ml aprotinin; 100 μM phenylmethylsulfonylfluroride), followed by sonication (25 W; 10 sec). The media and lysate were then analyzed for insulin content by mouse insulin RIA (Linco Research, Inc., St. Charles, MO) (4, 26).

RNA Analysis

The preproinsulin mRNA levels in islets were analyzed by the RNase protection assay, using the Direct lysis kit (Ambion, Inc., Austin, TX), as described previously (4). Essentially, RNA was protected by [^{32}P]uridine-labeled antisense RNA fragments corresponding to the coding region of preproinsulin, or to part of the GAPDH coding region (Ambion). Samples were resolved on denaturing 5% acrylamide/Tris-borate EDTA-buffered gels and analyzed by autoradiography.

An initial indication of the steady-state mRNA levels for certain ATGs and lysosomal membrane-associated proteins (LAMP-1 and -2) was by semiquantitative RT-PCR analysis following methodology previously described for isolated islets (51). Essentially, total RNA was extracted from freshly isolated islet preparations from individual Rab3A$^{+/+}$ or Rab3A$^{-/-}$ mice using RNAeasy kits (QIAGEN, Chatsworth, CA) followed by DNase digestion to remove any contaminating DNA. The RNA was then converted to cDNA (Ready-To-Go T-Primed First-Strand Kit, Amersham Pharmacia Biotech (Piscataway, NJ). These cDNAs were used as templates for PCRs using specific primers of annealing temperatures between 60–65 C in the presence of $MgCl_2$ and deoxynucleotide triphosphates. Amplification was generally between 24–28 cycles to be in the linear range. PCR products were resolved on agarose gels and quantified using PerkinElmer Optiquant Analysis Software (PerkinElmer, Wellesley, MA). The apparent mRNA levels were relative to β-actin mRNA control. The mouse nucleotide sequences of the primers used were as follows. Preproinsulin-1: TGGTGCACTTCCTACCCCT (forward), GCCTTA GTTGCAGTAGTTCTCC (reverse); Preproinsulin-2: CTGTGGATGCGCTTCCT (forward), TTGCAGTAGTTCTCCAGCTGGTA (reverse); β-actin: AGGCGGACTGTTACTGAGC (forward), AACACCTCAAACCACTCCC (reverse); ATG4: ATGGGAGTTGGCGAAGGCAAGTCTA (forward), CGTTAAAGTCTTCCTCCGTCTTAC (reverse); ATG5: CATCCACTGGAAGAATGACAG (forward), CATCCAGAGCTGCTTGTGGTCT (reverse); ATG6 (also known as beclin-1): ACTGGACACGAGCTTCAAGAT (forward), TTCCTCCTGGTCCAATCACA (reverse); ATG7: CAGCAAATGAGATCTGGGAAGCC (forward), GCTTTAGGACAATCTGGGCTA (reverse); ATG8 (also known as LC3): ATTACGTGAACATGAGCGAGC (forward), AGGAAGAGACTGCTCCTGAC (reverse); ATG10: TCGACACCACATGTGGGAA (forward), GGTGATGTGAGATATTGCAGTCCCA (reverse); ATG12: CCAAGGACTCATTGACTTCATC (forward), AATAGAGGTCCCCTGAATAAGC (reverse); ATG16: AGTCCTGGACATGATGGTGCGT (forward), TCTCTTCTGTGTGGTCTGAGGT (reverse); LAMP-1: GAAAATGTTTCTGACCCCAGCCT (forward), GTGTCATTTGGGCTGATGTTGAACGC (reverse); LAMP-2: CCATTGGATGTCATCTTTAAGTGC (forward), GTTGAAAGCTGAGCCATTAG (reverse).

To confirm the specific decrease in LAMP-2 expression in Rab3A$^{-/-}$ islets, a fluorescence-based quantitative real-time RT-PCR method was applied as previously described (34), using the same forward and reverse primers for β-actin, LAMP-1, and LAMP-2 mRNA.

Immunoprecipitation

For analysis of proinsulin biosynthesis, isolated mouse islets were preincubated at 37 C in 200 μl KRB/0.1% (wt/vol) BSA, containing basal 2.8 mM glucose for 60 min, and for a further 60 min at either basal 2.8 mM or stimulatory 16.7 mM glucose. The last 20 min of the incubation was carried out in the additional presence of 250 μCi/ml [^{35}S]methionine to monitor protein/proinsulin biosynthesis as described elsewhere (4, 50). Islets were washed then lysed in lysis buffer with sonication (10 sec/25 W), and the lysates were subjected to immunoprecipitation using guinea pig antibovine insulin (Sigma) as described previously (4, 50). Immunoprecipitated (pro)insulin was resolved by alkaline-urea gel electrophoresis. Gels were fixed in 50% methanol/10% acetic acid, dried, and quantified by phosphor imager analysis. Total protein synthesis was analyzed by 10% (wt/vol) trichloroacetic acid precipitation of 5 μl aliquots of the same islet lysates as described elsewhere (4, 50). The extent of specific glucose-induced proinsulin biosynthesis was corrected for the smaller effect of glucose on total protein synthesis.

For pulse-chase radiolabeling studies to examine proinsulin conversion, isolated mouse islets were incubated in batches of 50 at 37 C in 200 μl KRB/0.1% (wt/vol) BSA for 30 min at 16.7 mM glucose, and then for another 30-min pulse under the same conditions but in the presence of 250 μCi/ml [^{35}S]methionine. Islets were washed, and then chased for 0, 30, 60, 90, 120, or 180 min in 500 μl KRB/0.1% (wt/vol) BSA at 37 C containing 1 mM methionine at basal 2.8 mM glucose to minimize (pro)insulin secretion as previously established. At each chase time point, islets were collected, washed, lyzed by sonication, and subsequently immunoprecipitated for (pro)insulin, with [^{35}S]proinsulin/insulin processing analyzed by alkaline-urea gel electrophoresis as described above. For longer (pro)insulin degradation pulse-chase radiolabeling experiments a similar approach was taken, except that a longer 90-min pulse in the presence of 250 μCi/ml [^{35}S]methionine was used. In addition, as the chase incubation periods were much longer, these were conducted at 37 C in RPMI 1640 tissue culture medium (Invitrogen, Carlsbad, CA) containing 2.8 mM glucose, 10% fetal bovine serum (Hyclone Laboratories, Inc., Logan, UT), 100 U/ml penicillin, and 100 μg/ml streptomycin (Invitrogen) for 5, 24, 48, or 96 h, where the media was changed every 24 h.

High-Pressure Freezing and Freeze Substitution

After overnight culture in RPMI medium containing fetal bovine serum 10% (vol/vol) and 7 mM glucose (Sigma), islets were kept warm in culture medium buffered by the addition of HEPES (10 mM) on a humidified heating block at 37 C before freezing experiments. The sample holders used for high-pressure freezing experiments were also prewarmed to 37 C. Depending on size, 10–30 islets were gently manipulated into one half of the holder prefilled with HEPES-buffered RPMI containing fetal bovine serum 10% (vol/vol) and 7 mM glucose (Sigma). All manipulations were carried out on Parafilm placed on top of an inverted heating block warmed to 37 C under a dissecting microscope. The second half of the sample holder, filled with RPMI containing 10% dialyzed Ficoll (molecular mass, 70 kDa) and 0.5% Type IX ultra-low temperature gelling agarose (Sigma) as extracellular cryoprotectants, was then placed on top of the half of the sample holder containing the islets (32). Islets were frozen within approximately 10 msec under high pressure (~2100 atmospheres) using a Balzers HPM 010 high-pressure freezer (BAL-TEC AG, Liechtenstein, Germany) and stored under liquid nitrogen. Specimens were freeze substituted and plastic embedded essentially as described previously (31).

Microtomy and Microscopy

Ribbons of serial thin (40–60 nm) sections cut from plastic-embedded islets using a Leica UltraCut-UCT microtome (Leica, Inc., Deerfield, IL) and collected onto Formvar-coated copper slot grids were poststained with 2% aqueous uranyl acetate and Reynold's lead citrate to increase contrast when viewed in the EM. Grids were surveyed on a conventional electron microscope operating at 80 keV. Grids containing 300–400 nm-thick sections for tomographic analysis were

lightly carbon coated to minimize charging in the EM. Colloidal gold particles (10 or 15 nm) were deposited on both surfaces of these sections for use as fiducial markers during subsequent image alignment. Tilt series data were digitally recorded as the sample grid was serially tilted at 1.5° angular increments over a range of 120° (±60°) about two orthogonal axes, and dual-axis tomograms (3D reconstructions) were generated as detailed elsewhere (31, 32).

Statistical Analysis

Results are expressed as means ± SE. Statistical analysis was performed by unpaired Student's *t* test or repeated measure ANOVA, where $P < 0.05$ was considered significant.

Acknowledgments

We thank Thomas H. Giddings, Jr., for maintaining the core EM facilities in the Department of MCD Biology at the University of Colorado at Boulder, and J. Richard McIntosh and David Mastronarde, Directors of The Boulder Laboratory for 3D Electron Microscopy of Cells, for their professional and intellectual support throughout these studies.

Received February 9, 2007. Accepted June 15, 2007.

Address all correspondence and requests for reprints to: Christopher J. Rhodes, Kovler Diabetes Center, Department of Medicine, Section of Endocrinology, Diabetes, and Metabolism, University of Chicago, 5841 South Maryland Avenue, MC 1027, Room N138, Chicago, Illinois 60637. E-mail: cjrhodes@uchicago.edu.

The Boulder facility is supported by a National Institutes of Health (NIH) National Center for Research Resources (NCRR) Biomedical Technology Grant (P41 RR00592). This work was additionally supported by NIH Grants DK-47919 and DK-50610 (to C.J.R). B.J.M is supported by a Career Development Award from the Juvenile Diabetes Research Foundation International (2-2004-275).

Current Address for K.Y.: Department of Physiology and First Department of Internal Medicine, Kagoshima University School of Medicine, 8–35-1 Sakuragaoka, Kagoshima 890, Japan.

Disclosure Statement: B.J.M., C.S., C.A., B.L.W., K.Y., A.J.C., and G.P.M. have nothing to declare. C.J.R. has consulted for Amylin Pharmaceuticals, Inc./Eli Lilly partnership, Merck Inc., Takeda Pharmaceuticals Inc., and Metabolex Inc.

REFERENCES

1. Orci L 1985 The insulin factory: a tour of the plant surroundings and a visit to the assembly line. The Minkowski lecture 1973 revisited. Diabetologia 28:528–546
2. Rorsman P, Renstrom E 2003 Insulin granule dynamics in pancreatic β-cells. Diabetologia 46:1029–1045
3. Rhodes CJ 2004 Processing the insulin molecule. In: LeRoith D, Taylor SI, Olefsky JM, eds. Diabetes mellitus a fundamental and clinical text. 3rd ed. Philadelphia: Lippincott-Raven Publishers; 27–50
4. Wicksteed B, Alarcon C, Briaud I, Lingohr MK, Rhodes CJ 2003 Glucose-induced translational control of proinsulin biosynthesis is proportional to preproinsulin mRNA levels in islet β-cells but not regulated via a positive feedback of secreted insulin. J Biol Chem 278: 42080–42090
5. Ashcroft SJ 1980 Glucoreceptor mechanisms and the control of insulin release and biosynthesis. Diabetologia 18:5–15
6. Halban PA 1991 Structural domains and molecular lifestyles of insulin and its precursors in the pancreatic β cell. Diabetologia 34:767–778
7. Halban PA, Wollheim CB 1980 Intracellular degradation of insulin stores by rat pancreatic islets in vitro. An alternative pathway for homeostasis of pancreatic insulin content. J Biol Chem 255:6003–6006
8. Orci L, Ravazzola M, Amherdt M, Yanaihara C, Yanaihara N, Halban P, Renold AE, Perrelet A 1984 Insulin, not C-peptide (proinsulin), is present in crinophagic bodies of the pancreatic B-cell. J Cell Biol 98:222–228
9. Bommer G, Schafer HJ, Kloppel G 1976 Morphologic effects of diazoxide and diphenylhydantoin on insulin secretion and biosynthesis in B cells of mice. Virchows Arch A Pathol Anat Histol 371:227–241
10. Skoglund G, Ahren B, Lundquist I 1987 Biochemical determination of islet lysosomal enzyme activities following crinophagy-stimulating treatment with diazoxide in mice. Diabetes Res 6:81–84
11. Dunn WA, Jr. 1994 Autophagy and related mechanisms of lysosome-mediated protein degradation. Trends Cell Biol 4:139–143
12. Yoshimori T 2004 Autophagy: a regulated bulk degradation process inside cells. Biochem Biophys Res Commun 313:453–458
13. Stromhaug PE, Klionsky DJ 2001 Approaching the molecular mechanism of autophagy. Traffic 2:524–531
14. Klionsky DJ, Emr SD 2000 Autophagy as a regulated pathway of cellular degradation. Science 290:1717–1721
15. Wang CW, Klionsky DJ 2003 The molecular mechanism of autophagy. Mol Med 9:65–76
16. Cuervo AM 2004 Autophagy: in sickness and in health. Trends Cell Biol 14:70–77
17. Halban PA, Mutkoski R, Dodson G, Orci L 1987 Resistance of the insulin crystal to lysosomal proteases: implications for pancreatic B-cell crinophagy. Diabetologia 30:348–353
18. Farquhar MG 1977 Secretion and crinophagy in prolactin cells. Adv Exp Med Biol 80:37–94
19. Schnell AH, Swenne I, Borg LA 1988 Lysosomes and pancreatic islet function. A quantitative estimation of crinophagy in the mouse pancreatic B-cell. Cell Tissue Res 252:9–15
20. Borg LA, Schnell AH 1986 Lysosomes and pancreatic islet function: intracellular insulin degradation and lysosomal transformations. Diabetes Res 3:277–285
21. Landstrom AH, Westman J, Borg LA 1988 Lysosomes and pancreatic islet function. Time course of insulin biosynthesis, insulin secretion, and lysosomal transformation after rapid changes in glucose concentration. Diabetes 37:309–316
22. Schnell Landstrom AH, Andersson A, Borg LA 1991 Lysosomes and pancreatic islet function: adaptation of β-cell lysosomes to various metabolic demands. Metabolism 40:399–405
23. Geppert M, Bolshakov VY, Siegelbaum SA, Takei K, De Camilli P, Hammer RE, Sudhof TC 1994 The role of Rab3A in neurotransmitter release. Nature 369:493–497
24. Donelan MJ, Morfini G, Julyan R, Sommers S, Hays L, Kajio H, Briaud I, Easom RA, Molkentin JD, Brady ST, Rhodes CJ 2002 Ca2+-dependent dephosphorylation of kinesin heavy chain on β-granules in pancreatic β-cells. Implications for regulated β-granule transport and insulin exocytosis. J Biol Chem 277:24232–24242
25. Rhodes CJ, Halban PA 1987 Newly synthesized proinsulin/insulin and stored insulin are released from pancreatic B cells predominantly via a regulated, rather than a constitutive, pathway. J Cell Biol 105:145–153
26. Yaekura K, Julyan R, Wicksteed BL, Hays LB, Alarcon C, Sommers S, Poitout V, Baskin DG, Wang Y, Philipson LH, Rhodes CJ 2003 Insulin secretory deficiency and glucose intolerance in Rab3A null mice. J Biol Chem 278:9715–9721

27. Drucker DJ 2001 Minireview: the glucagon-like peptides. Endocrinology 142:521–527
28. Hodgkin DC 1974 Proceedings: varieties of insulin. The Sir Henry Dale lecture for 1974. J Endocrinol 63:3P–14P
29. Greider MH, Howell SL, Lacy PE 1969 Isolation and properties of secretory granules from rat islets of Langerhans. II. Ultrastructure of the β granule. J Cell Biol 41:162–166
30. Erlandsen SL 1980 Types of pancreatic islet cells and their immunocytochemical identification. Monogr Pathol 21:140–155
31. Marsh BJ, Mastronarde DN, Buttle KF, Howell KE, McIntosh JR 2001 Organellar relationships in the Golgi region of the pancreatic β cell line, HIT-T15, visualized by high resolution electron tomography. Proc Natl Acad Sci USA 98:2399–2406
32. Marsh BJ, Volkmann N, McIntosh JR, Howell KE 2004 Direct continuities between cisternae at different levels of the Golgi complex in glucose-stimulated mouse islet β cells. Proc Natl Acad Sci USA 101:5565–5570
33. Shintani T, Klionsky DJ 2004 Autophagy in health and disease: a double-edged sword. Science 306:990–995
34. Alarcon C, Wicksteed B, Rhodes CJ 2006 Exendin 4 controls insulin production in rat islet β cells predominantly by potentiation of glucose-stimulated proinsulin biosynthesis at the translational level. Diabetologia 49: 2920–2929
35. Tanaka Y, Guhde G, Suter A, Eskelinen EL, Hartmann D, Lullmann-Rauch R, Janssen PM, Blanz J, von Figura K, Saftig P 2000 Accumulation of autophagic vacuoles and cardiomyopathy in LAMP-2-deficient mice. Nature 406: 902–906
36. Eskelinen EL 2006 Roles of LAMP-1 and LAMP-2 in lysosome biogenesis and autophagy. Mol Aspects Med 27:495–502
37. Eskelinen EL, Tanaka Y, Saftig P 2003 At the acidic edge: emerging functions for lysosomal membrane proteins. Trends Cell Biol 13:137–145
38. Kitiphongspattana K, Mathews CE, Leiter EH, Gaskins HR 2005 Proteasome inhibition alters glucose-stimulated (pro)insulin secretion and turnover in pancreatic β-cells. J Biol Chem 280:15727–15734
39. Dunn Jr WA 1990 Studies on the mechanisms of autophagy: maturation of the autophagic vacuole. J Cell Biol 110:1935–1945
40. Farquhar MG 1981 Membrane recycling in secretory cells: implications for traffic of products and specialized membranes within the Golgi complex. Methods Cell Biol 23:399–427
41. Straub SG, Shanmugam G, Sharp GW 2004 Stimulation of insulin release by glucose is associated with an increase in the number of docked granules in the β-cells of rat pancreatic islets. Diabetes 53:3179–3183
42. Levine B, Klionsky DJ 2004 Development by self-digestion: molecular mechanisms and biological functions of autophagy. Dev Cell 6:463–477
43. Nishino I, Fu J, Tanji K, Yamada T, Shimojo S, Koori T, Mora M, Riggs JE, Oh SJ, Koga Y, Sue CM, Yamamoto A, Murakami N, Shanske S, Byrne E, Bonilla E, Nonaka I, DiMauro S, Hirano M 2000 Primary LAMP-2 deficiency causes X-linked vacuolar cardiomyopathy and myopathy (Danon disease). Nature 406:906–910
44. Gonzalez-Polo RA, Boya P, Pauleau AL, Jalil A, Larochette N, Souquere S, Eskelinen EL, Pierron G, Saftig P, Kroemer G 2005 The apoptosis/autophagy paradox: autophagic vacuolization before apoptotic death. J Cell Sci 118:3091–3102
45. Luzio JP, Poupon V, Lindsay MR, Mullock BM, Piper RC, Pryor PR 2003 Membrane dynamics and the biogenesis of lysosomes. Mol Membr Biol 20:141–154
46. Mullins C, Bonifacino JS 2001 The molecular machinery for lysosome biogenesis. Bioessays 23:333–343
47. Jager S, Bucci C, Tanida I, Ueno T, Kominami E, Saftig P, Eskelinen EL 2004 Role for Rab7 in maturation of late autophagic vacuoles. J Cell Sci 117:4837–4848
48. Lupi R, Dotta F, Marselli L, Del Guerra S, Masini M, Santangelo C, Patane G, Boggi U, Piro S, Anello M, Bergamini E, Mosca F, Di Mario U, Del Prato S, Marchetti P 2002 Prolonged exposure to free fatty acids has cytostatic and pro-apoptotic effects on human pancreatic islets: evidence that β-cell death is caspase mediated, partially dependent on ceramide pathway, and Bcl-2 regulated. Diabetes 51:1437–1442
49. Rhodes CJ 2005 Type 2 diabetes-a matter of β-cell life and death? Science 307:380–384
50. Alarcón C, Lincoln B, Rhodes CJ 1993 The biosynthesis of the subtilisin-related proprotein convertase PC3, but not that of the PC2 convertase, is regulated by glucose in parallel to proinsulin biosynthesis in rat pancreatic islets. J Biol Chem 268:4276–4280
51. Kulkarni RN, Holzenberger M, Shih DQ, Ozcan U, Stoffel M, Magnuson MA, Kahn CR 2002 β-cell-specific deletion of the Igf1 receptor leads to hyperinsulinemia and glucose intolerance but does not alter β-cell mass. Nature genetics 31:111–115